INTERFACE

rsif.royalsocietypublishing.org

Research

Cite this article: Popescu DM, Sun SX. 2018 Building the space elevator: lessons from biological design. *J. R. Soc. Interface* **15**: 20180086.
http://dx.doi.org/10.1098/rsif.2018.0086

Received: 5 February 2018
Accepted: 21 September 2018

Subject Category:
Life Sciences – Engineering interface

Subject Areas:
biocomplexity

Keywords:
space elevator, biological design, age-structured dynamics

Author for correspondence:
Sean X. Sun
e-mail: ssun@jhu.edu

THE ROYAL SOCIETY PUBLISHING

Building the space elevator: lessons from biological design

Dan M. Popescu[1] and Sean X. Sun[2,3]

[1]Department of Applied Mathematics and Statistics, [2]Department of Mechanical Engineering, and [3]Department of Biomedical Engineering, Johns Hopkins University, Baltimore, MD 21218, USA

SXS, 0000-0002-9077-7088

One of the biggest perceived challenges in building megastructures, such as the space elevator, is the unavailability of materials with sufficient tensile strength. The presumed necessity of very strong materials stems from a design paradigm which requires structures to operate at a small fraction of their maximum tensile strength (usually, 50% or less). This criterion limits the probability of failure by giving structures sufficient leeway in handling stochastic components, such as variability in material strength and/or external forces. While reasonable for typical engineering structures, low working stress ratios—defined as operating stress as a fraction of ultimate tensile strength—in the case of megastructures are both too stringent and unable to adequately control the failure probability. We draw inspiration from natural biological structures, such as bones, tendons and ligaments, which are made up of smaller substructures and exhibit self-repair, and suggest a design that requires structures to operate at significantly higher stress ratios, while maintaining reliability through a continuous repair mechanism. We outline a mathematical framework for analysing the reliability of structures with components exhibiting probabilistic rupture and repair that depend on their time-in-use (age). Further, we predict time-to-failure distributions for the overall structure. We then apply this framework to the space elevator and find that a high degree of reliability is achievable using currently existing materials, provided it operates at sufficiently high working stress ratios, sustained through an autonomous repair mechanism, implemented via, e.g. robots.

1. Introduction

Once an element of science fiction, the space elevator has become in recent years one of the most ambitious and grandiose engineering projects. Although the concept of a space elevator was introduced by Russian physicist Konstantin Tsiolkovsky in 1895 [1], the idea goes back to biblical times when the attempt to create a tower to heaven (later named 'The Tower of Babel') ended in ruin. In the late 1990s, NASA considered the idea rigorously and concluded that such a massive structure is not only feasible, but is a cost-efficient way to transport payloads into space [2]. A few years later, two NASA Institute of Advanced Science (NIAC) reports outlined various engineering considerations to building the megastructure [3,4]. The reports emphasized the necessity of extremely strong materials, but the dawn of carbon nanotubes dispelled some of the scepticism in the scientific community. Currently, commercial companies planning on building the elevator are on hold, awaiting advancements in materials science.

In this paper, we argue that a key concept needed for building megastructures like the space elevator can be borrowed from biology. On a much smaller scale, living organisms can be viewed as megastructures when compared to their building blocks (e.g. tendons composed of collagen fibres, bones made of osteons, etc.). So how does biological design create such stable structures? The answer is not only to maximize the strength of the materials used, but also to

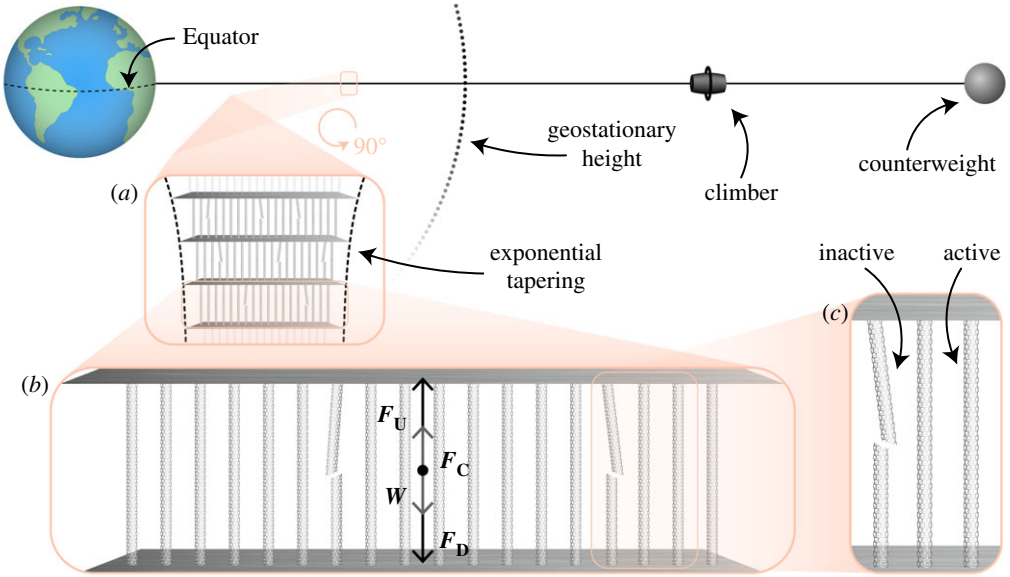

Figure 1. Space elevator diagram. (*a*) The space elevator tether is anchored at the Equator, extends past geostationary orbit and is balanced by a counterweight. The tether is made up of independent horizontal segments stacked vertically. Each segment is made up of filaments. The number of filaments for each segment varies exponentially with height. (*b*) A tether segment experiences four forces: its weight $\boldsymbol{W}$, the outward centrifugal force $\boldsymbol{F_C}$, and upward/downward forces $\boldsymbol{F_U}$ and $\boldsymbol{F_D}$, owing to the part of the cable above/below the element. At equilibrium, $\boldsymbol{F_U} + \boldsymbol{F_C} = \boldsymbol{W} + \boldsymbol{F_D}$, leading to tension in the bundle. (*c*) Segment filaments are active if they carry load. Otherwise, they are inactive. Active segments can become inactive through rupture and inactive cables can become active through repair.

cheaply repair by recycling material, while operating at very high loads. Although it is a good rule of thumb in reliability engineering to have structures with a maximum safety factor—that is, how much load the part can withstand versus actual or expected load—of 2, biological systems operate significantly below this value. For example, in humans, Achilles' tendons experience safety factors well below 1.5, routinely withstanding mechanical stresses very close to their ultimate tensile strengths (UTSs) [5]. Similarly, lumbar spines in humans can also sustain tremendous stresses, especially in athletes [6]. As Taylor *et al*. [7] point out, the key to sustainability lies in the repair mechanism inherent in biological systems.

Incidentally, engineering has a long history of borrowing from biology dating back to classic civilizations' use of ballistae, which used twisted tendons to accelerate projectiles on account of the little weight they would add to the machine [8]. In the same spirit, we suggest a megastructure design that not only allows components to fail, but has a self-repair mechanism to replace the broken components. This will allow structures to operate at significantly higher loads, without compromising their integrity, which, in turn, will make megastructures built from existing materials a reality.

The physics of the space elevator as a balanced tether extending from the Equator past geosynchronous height has been previously studied [9–11]. In the rotating frame of the Earth's surface, the tether is freestanding—that is, it exerts no force on the ground—if its weight and outward centrifugal force are in balance, thus maintaining it under lengthwise tension. Using the notation in [11], figure 1*b* shows that each small, horizontal element of the tether experiences four forces: its weight $\boldsymbol{W}$, the outward centrifugal force $\boldsymbol{F_C}$ and upward/downward forces $\boldsymbol{F_U}$ and $\boldsymbol{F_D}$, owing to the part of the cable above/below the element (and a potential counterweight placed above geosynchronous height to reduce the cable length needed). A balanced tether implies that, each segment is in equilibrium in the aforementioned rotating frame of reference, that is, $\boldsymbol{F_U}$. Note that, $\boldsymbol{W} = \boldsymbol{F_C}$ (and $\boldsymbol{F_U} = \boldsymbol{F_D}$) at geostationary height, $\boldsymbol{W} > \boldsymbol{F_C}$ (and $\boldsymbol{F_U} > \boldsymbol{F_D}$) below and the reverse is true for an element above this height.

Pearson suggested that a desirable design is to maintain a constant stress σ throughout the tether [10]. Then, for an element below geostationary orbit, we have $\boldsymbol{F_U} - \boldsymbol{F_D} = \sigma \mathrm{d}A = \boldsymbol{W} - \boldsymbol{F_C}$, where A is the cross-sectional area of the cable. This results in an exponential tapering of A shown schematically in figure 1*a*: A increases from a small value at the base to a large one at geostationary height and back to a small one thereafter. The taper ratio—defined as area at geostationary height divided by area at the Earth's surface—is given by $T = \exp(K/L_c)$. Here, K is a constant that depends on Earth's radius and geostationary height and $L_c = \sigma/w$ is the characteristic length of the material, i.e. the ratio between the constant stress in the tower σ and the specific weight w. It can be seen that, to avoid prohibitively large cross-sectional areas, one should use light (small w) materials able to sustain high stresses (large σ). For reference, using a safety factor of 2, a steel cable requires a taper ratio $T = 2.6 \times 10^{66}$, whereas for carbon nanotubes, assuming a maximum tensile strength of 130 GPa, the taper ratio is $T = 2.6$ (table 1). These extreme requirements make carbon nanotubes a natural choice. However, with lengths not exceeding several centimetres [12,14], using them in their raw form to build the space elevator is not feasible. A solution is to use carbon nanotube composites [4], but this decreases their tensile properties. Some of the strongest carbon nanotube composites currently available have maximum tensile strengths of 25–31 GPa [15,16], highlighting we are fast approaching the material strength ranges necessary for stable megastructures with self-repair mechanisms.

2. Filament bundle rupture dynamics with repair

2.1. Space elevator model

Although the finished space elevator may comprise enough parallel tethers (cables) to meet cargo transport demands

Table 1. Space elevator characteristics for different materials. (We show material specific weight, ultimate tensile strength (UTS), and cable taper ratio, total mass and number of flights required to transport the material for two different operating stress ratios ω. Data for steel, Kevlar and CNT (theoretical) is adapted from Aravind [11], data for CNT (STR method) from [12], Zylon and M5 data from [13]. The number of flights is estimated based on Pearson [10].)

			taper ratio, T		mass (tonnes)		no. of flights	
material	sp. weight (kN m^{-3})	UTS (GPa)	$\omega = 50\%$	$\omega = 100\%$	$\omega = 50\%$	$\omega = 100\%$	$\omega = 50\%$	$\omega = 100\%$
steel	77	5.0	3.4×10^{66}	1.8×10^{33}	5.9×10^{68}	2.3×10^{35}	2.5×10^{65}	9.5×10^{31}
Kevlar	14	3.6	7.0×10^{16}	2.6×10^{8}	6.0×10^{18}	1.6×10^{10}	1.4×10^{16}	3.7×10^{7}
Zylon	15	5.8	2.1×10^{11}	4.6×10^{5}	1.5×10^{13}	2.3×10^{7}	3.2×10^{10}	4.9×10^{4}
M5	17	7.2	8.8×10^{9}	9.4×10^{4}	5.8×10^{14}	4.3×10^{9}	1.1×10^{9}	8.5×10^{3}
CNT (STR)	16	43.0	36.9	6.1	837.5	81.2	1.7	0.2
CNT (th.)	13	130.2	2.6	1.6	20.8	6.8	5.3×10^{-2}	1.7×10^{-2}

[3,4], we focus here on the first cable. Specifically, we model each tether as a set of vertically stacked segments (figure 1); each segment is made up of identical, parallel, non-interacting filaments. We assume idealized, indestructible connections between the segments, but one can envision an extension to the model where the connections are treated as a second type of segment with their own dynamics. The total number of segments is determined by the maximum filament length and the amount of stress variation permitted in the segment (gravitational forces acting on segments vary with height). To maintain a tapered shape of the cable, each segment's cross-sectional area changes with height by varying the (target) numbers of filaments in the segment, effectively obtaining a step-wise discretized version of the continuous exponential tapering discussed above.

We further restrict the analysis to a single segment shown schematically in figure 1*b*. Filaments in the segment are *active* if supporting load and *inactive* if broken and not sustaining load. Additionally, active filaments can fail and become inactive and, conversely, inactive filaments are repaired by replacing them with active ones. We assume the processes of rupture and repair do not significantly change the mass of the segment. Furthermore, the segment height is considered small enough to ignore variability in gravity and centrifugal forces. Therefore, the net force on the segment is constant and, hence, segment dynamics are independent of the dynamics of its neighbours. The independence ensures that the failure probability of the cable is the probability that any of its segments fail; if the latter is controlled and arbitrarily small, the former can be too. When filaments are gained or lost, the resulting load is instantaneously divided among all active filaments. We ignore the interaction between filaments (e.g. friction) and changes in the inter-filament platform angles. However, the model is flexible enough to incorporate aspects discussed in [4], such as a ribbon pattern to protect against potential hazards (e.g. by changing segment orientation). We point out that the model also mirrors biological structures built with smaller subunits. For example, tendons and parallel collagen fibrils, which, with the help of tendocytes that actively synthesize matrix components provide a self-repair mechanism [17]. A similar mechanism is present in bones, where osteoclasts and osteoblasts form basic multicellular units that move along the bone and turnover material [7].

The segment-filament model proposed here is a simplified model for gaining intuition about the structure–substructure interaction, rather than a suggestion for a specific engineering design. In the case of no repair, our non-interacting filament model is known as the *equal load sharing fibre bundle model*. This has been studied extensively in the literature, beginning with Daniels [18], who analysed bundle strength in fast rupture and Coleman [19–21], who worked on fibre bundle lifetime in time-dependent creep-rupture, with further generalizations by Phoenix [22,23]. Past analytic work is restricted to the case where fibre rupture times are exponentially distributed, leading to a memoryless Markov process (see §3.5) and involves 'mean-field' approaches, as well as asymptotics for large number of fibres, where fluctuations can be ignored. Newman and Phoenix's more recent work [24,25] explores simulation algorithms for large number of fibres in the case of local load sharing breakage for more general underlying fibre lifetime distributions. The analytic approach used in our paper does not impose restrictions on the underlying filament lifetime distributions, can be solved exactly, and, more importantly, extends to the case where filaments are repaired, a case where the age-structure of the ensemble becomes crucial. We emphasize our analysis combines the deterministic aspect of ageing with the stochastic rupture/repair of the filaments.

2.2. Dynamics of active filaments

As underlined in the model description, the goal is to maintain a constant stress throughout the structure, which translates to maintaining a constant stress for each segment in the steady state. Assuming a sufficiently large number of segments, the total force in each is constant. Then, in the transition phase, one expects changes in the single segment stress owing solely to variations in its cross-sectional area. This area is the product between $n(t)$—the number of active filaments at time t—and the constant cross-sectional area of a single filament. Equivalently, the product $\sigma(t) \times n(t)$ is constant, where σ is the stress in the segment at time t. The segment is considered operational if $\sigma(t) < \sigma_{\max}$, with $\sigma_{\max}$ a constant representing the UTS of the material. It is more convenient to view this inequality in terms of the *working stress ratio*, which we define as $\omega(t) := \sigma(t)/\sigma_{\max}$. Then, the condition for reliability of the structure becomes $\omega(t) < 100\%$. Note that, designing a structure with a specific safety factor corresponds in our language to targeting a fixed value for ω.

When considering the dynamics of $\omega(t)$, it is more direct to analyse $n(t)$, the number of active filaments. We assume

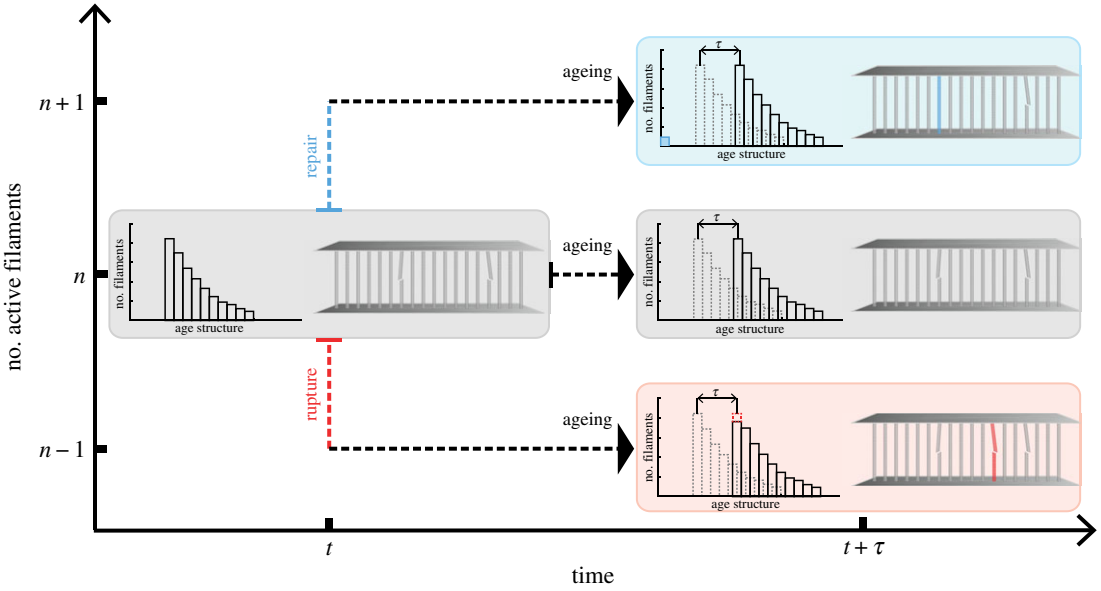

Figure 2. Stochastic bundle model with ageing. At time t, there are n active filaments. The ith active filament has age a_i, measured from the time of its loading. Ages can differ among filaments owing to the repair process, according to which inactive filaments are replaced with active ones. Each filament has a rupture probability rate $k_n(a_i)$, which depends on the specific filament's age a_i. The whole system has a probability rate of repair given by ρ_n. During each small increment of time τ, the system ages deterministically by τ, shifting the overall age distribution ($a_i \longrightarrow a_i + \tau$) and also jumps stochastically to one of three states: (i) $n-1$ filaments (rupture, red) with probability $\sum_{i=1}^{n} \int_0^{\tau} k_n(a_i + \tau')\,\mathrm{d}\tau'$, (ii) $n+1$ (repair, blue) with probability $\rho_n \tau$, or (iii) n filaments (grey) with probability $1 - (\rho_n \tau + \sum_{i=1}^{n} \int_0^{\tau} k_n(a_i + \tau')\,\mathrm{d}\tau'))$.

there are two *stochastic* effects which govern the kinetics of $n(t)$: filament *rupture* and *repair*. Filament rupture times are, therefore, random variables drawn from a lifetime distribution, which depends on the stress (load history) $\sigma(t)$ (or, equivalently, on $n(t)$). A typical choice for this distribution is Weibull [26–29]. Since new filaments are introduced in the system through the repair process at various times, we denote by a_i the ith active filament's age—the time elapsed from the moment it begins bearing load. Each filament therefore has a rupture rate of $k_n(a_i)$. On the other hand, we assume that filaments are autonomously repaired by robots with a piecewise-constant probability per unit time ρ_n (see §2.3 for a detailed discussion on the transition probability rates).

The dynamics of $n(t)$ are represented schematically in figure 2. During any small increment of time τ, either an active filament ruptures ($n \to n-1$) according to $k_n(a)$, or an inactive one is repaired according to ρ_n ($n \to n+1$), or neither. In either case, *all* loaded filaments will age deterministically, shifting the age-structure of active filaments. We can describe this process mathematically in the formalism of Chou & Greenman [30,31]. If we *randomly* label the filaments $1, 2, \ldots, n$, we let $p_n(\boldsymbol{a}_n; t)\,\mathrm{d}\boldsymbol{a}_n$ be the probability that the ith one has age in the interval $[a_i,\ a_i + \mathrm{d}a_i]$, where $\boldsymbol{a}_n = (a_1, a_2, \ldots, a_n)$ is the vector of ages. We can then write the hierarchy of coupled integro-differential equations as:

$$\overbrace{\underbrace{\frac{\partial p_n(\boldsymbol{a}_n; t)}{\partial t}}_{\text{change due to time}} + \underbrace{\sum_{i=1}^{n} \frac{\partial p_n(\boldsymbol{a}_n; t)}{\partial a_i}}_{\text{change due to ageing}}}^{\text{total change in probability}} = \overbrace{-p_n(\boldsymbol{a}_n; t) \sum_{i=1}^{n} k_n(a_i)}^{\text{probability outflux due to rupture}}$$
$$\underbrace{+ (n+1) \int_0^{\infty} k_{n+1}(\alpha) p_{n+1}(\boldsymbol{a}_n, \alpha; t) d\alpha}_{\text{probability influx due to rupture}}, \tag{2.1}$$

with the associated boundary condition $n p_n(\boldsymbol{a}_{n-1}, 0; t) = \rho_n p_{n-1}(\boldsymbol{a}_{n-1}; t)$, which embeds the effect of repair. In addition to the boundary conditions, one needs to also provide an initial condition $p_n(\boldsymbol{a}_n; t = 0)$ to fully specify the system. Integrating over all ages $\boldsymbol{a}_n$, one gets the probability of having $n(t)$ active filaments at time t, that is, $p(n, t) = \int p_n(\boldsymbol{a}_n; t)\,\mathrm{d}\boldsymbol{a}_n$. This hierarchy leads to an exact analytic solution for the probability density, albeit an unwieldy one [31].

2.3. Derivation of the transition probabilities

2.3.1. Rupture

There are various modes in which mechanical structures can fail (e.g. ductile fracture, brittle fracture, fatigue, etc.) [32]. In this manuscript, we focus exclusively on creep-rupture—the time-dependent deformation process under moderate to high stresses. Our decision is justified given the tapered design of the space elevator cable, which implies a high constant stress throughout the structure. It is interesting to note that creep-rupture data turns out to be far from abundant for low temperatures. This is somewhat expected given that the stresses involved in obtaining reasonable times to rupture in relevant materials are typically significantly above 50% of their UTSs. Since most engineering structures are designed to operate below these stress ratios, research in this area is somewhat scarce.

To obtain the probability of failure owing to creep-rupture, it is reasonable to assume that filament rupture time is distributed according to a Weibull distribution [26–29]. We highlight that the inferences drawn regarding the trade-off between repair rates and sustaining higher stresses do not change meaningfully depending on the choice of distributions; we are limiting the analysis to Weibull for the sake of definiteness. We seek the conditional probability that a filament ruptures in an interval of time τ, given that it has been in use a time of a_i, i.e. has age a_i. We let $F_W(a_i)$ be the Weibull probability of rupture in the interval $[0,\ a_i]$ in

equation (4.1) and $f_W(a_i) = F'_W(a_i)$ its associated probability density function. If τ is small, the probability of rupturing during $[a_i, a_i + \tau]$ is $f_W(a_i)\tau$. The probability that the filament reached age a_i unruptured is $1 - F_W(a_i)$. The conditional probability per unit time (transition probability rate) is then

$$k(a_i; \lambda, s) = \lim_{\tau \to 0} \frac{1}{\tau} \frac{f_W(a_i)\tau}{1 - F_W(a_i)} = \frac{s}{\lambda^s} a_i^{s-1}. \tag{2.2}$$

Note that, $k(\cdot)$ is synonymous to the hazard function in survival analysis. We assume the shape parameter s is a constant and that a linear relationship of the form $\ln(\lambda) = \alpha \ln(\sigma) + \beta$ exists between the scale parameter λ and the stress σ (see §4 for details). Recalling that the total segment force is assumed constant and, hence, $\sigma(t) \times n(t)$ is constant, we can express the rupture rate as

$$k_n(a_i) = c_1 \left(\frac{n}{c_2}\right)^{\alpha s} a_i^{s-1}, \tag{2.3}$$

where c_1 is a constant that depends solely on material properties (see §4) and $c_2 = \sigma_0 N_0$ is a segment-specific constant, where σ_0 and N_0 are the initial stress and number of active filaments for the segment, respectively. For a detailed discussion on the choice of N_0, see §3.3.

2.3.2. Repair

The repair mechanism in this manuscript is independent of the filament age distribution:

$$\rho_n = \begin{cases} \rho & (n < N_0) \\ 0 & (n \geq N_0). \end{cases} \tag{2.4}$$

Here, ρ is a constant and N_0 is the initial number of active filaments. Provided the number of active filaments $n < N_0$, during every small time increment τ, there is a probability $\rho\tau$ for the entire segment to be repaired. The repair amounts to adding an active filament and removing an inactive one, thus leaving mass unchanged. Therefore, in this simplified case, the probability rate per unit time is a constant ρ. Alternatively, ρ filaments will be added on average per unit time. To continue the biological analogy, we can envision a mechanism that performs repairs automatically (e.g. autonomous robots). Given robots' arbitrary positions along the cable, each segment has a certain probability of getting repaired. The trade-off in adding more repairing robots comes from the added mass associated with them. However, we can also consider the control problem associated with picking more complex functional forms for the repair rate to potentially minimize material flux and total robot mass. It turns out that, despite being overly-conservative and choosing ρ as constant, the repair rate value is reasonable and structures can operate reliably at higher stresses.

2.4. Age-dependent stochastic simulation

In the case in which the rupture rates $k_n(a_i)$ depend on the number of active filaments n, the hierarchy in (2.1) leads to a somewhat unwieldy analytic solution. We use an age-dependent stochastic simulation method based on the time-dependent Gillespie algorithm [33], which takes into account the age structure of the population. Starting with N_0 filaments (see §3.3 for the choice of N_0), the algorithm generates a transition at every step of the iteration either until a passage condition is reached (e.g. the number of filaments drops below a critical value corresponding to $\omega = 100\%$) or a maximum number of iterations condition is reached. Each transition is broken down into two steps: finding the time to the first transition and determining which transition occurs.

Tackling the first step requires knowing the distribution of jump times. Let τ be the interval of time such that given a jump occurs at t, then the next jump will occur at $t + \tau$. Assume there are n filaments after the jump at t with ages $\boldsymbol{a}_n$. We are interested in the cumulative distribution of τ denoted $F_{n \to n \pm 1}(\tau \mid \boldsymbol{a}_n; t)$. First, focus on the probability that in the interval $[t, t + \tau]$ there occur no jumps. To derive this, we break up the interval τ into q small sub-intervals of size $\Delta\tau$. Using the definition of transition probabilities, we can write the probability that no transitions occur in $[t + l\Delta\tau, t + (l+1)\Delta\tau]$ for $l = 0, \ldots, q-1$ as $1 - [\rho + \sum_{i=1}^{n} k_n(a_i + l\Delta\tau)]\Delta\tau$. Since $\Delta\tau$ is chosen sufficiently small, we can write the probability as $\exp\{-\int_{l\Delta\tau}^{(l+1)\Delta\tau} [\rho + \sum_{i=1}^{n} k_n(a_i + \tau')]\, \mathrm{d}\tau'\}$. Taking the product over all $l = 0, \ldots, q$, we get the probability that no transition occurs on any of the sub-intervals. Then,

$$F_{n \to n \pm 1}(\tau \mid \boldsymbol{a}_n; t) = 1 - \exp\left\{-\left[\rho\tau + \sum_{i=1}^{n} \int_0^{\tau} k_n(a_i + \tau')\, \mathrm{d}\tau'\right]\right\}. \tag{2.5}$$

We draw R, a uniform random number on [0, 1] and find the jump time τ^* as the solution to the equation $F_{n \to n \pm 1}(\tau^* \mid \boldsymbol{a}_n; t) = R$ via the Newton–Raphson method.

The second step of the transition is to determine whether one of the n filaments ruptures or the segment is repaired. To accomplish this, we sample the categorical (multinomial with one trial) distribution, where each category has (unscaled) probability ρ, $k_n(a_1 + \tau^*)$, $k_n(a_2 + \tau^*)$, …, $k_n(\boldsymbol{a}_n + \tau^*)$ (only include a category for repair if $n < N_0$).

Once a transition occurs, the vector of ages $\boldsymbol{a}_n$ is incremented by τ^* component-wise. If the filament is broken, it leaves the pool and is no longer tracked. If the segment is repaired, a new filament with age $a_{\min}$ enters the pool. If no stopping conditions are met (e.g. barriers, maximum time), the algorithm continues to generate transitions.

3. Results

For the sake of concreteness, we focused on a space elevator segment built out of aramid filaments (see data analysis in §4). We first apply the classical reliability engineering paradigm of no autonomous repair to the space elevator and analyse the reliability of a segment. Without repair, a typical way of ensuring structure integrity is by designing it to operate at low working stress ratios ω (or, conversely, at high safety factors). This is a good rule of thumb when the distributions of material properties are well studied and stresses in the structure are low enough to allow for high safety factors. In the space elevator, however, high safety factors are unrealistic, as these would lead to exponential increases in the taper ratio [3]. Furthermore, while ductile materials, such as steel, have well-understood tensile properties, carbon nanotubes (most realistic material to be used for the space elevator) were shown to have considerably variable strengths [34]. Their brittle nature [35], coupled with the practical limits imposed on the safety factor, led us to suggest a paradigm shift from low

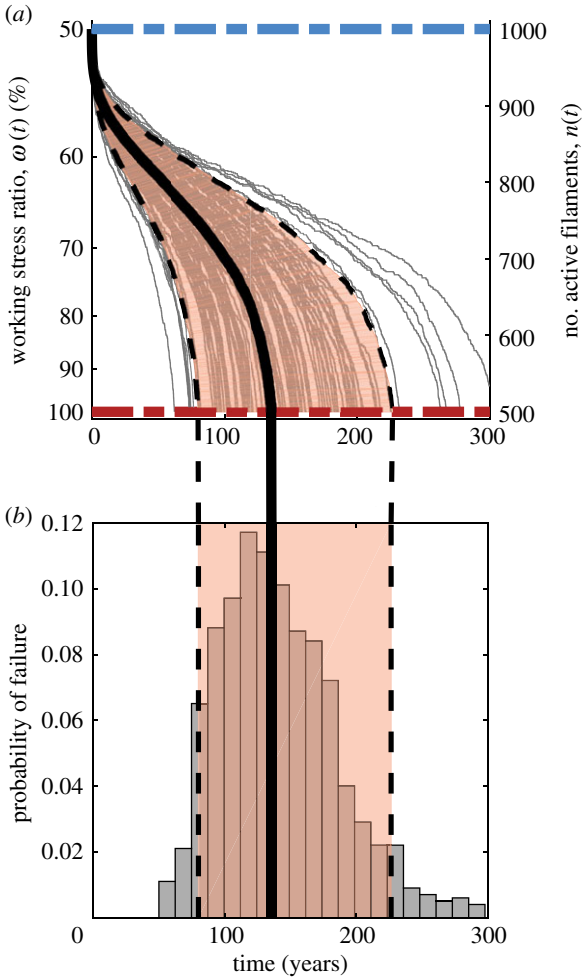

Figure 3. Dynamics without filament repair. (*a*) A sample of 100 paths (grey) are shown for the number of filaments $n(t)$ (right) and corresponding working stress ratio $\omega(t) := \sigma(t)/\sigma_{max}$ (left). The blue and red dashed lines show the initial working stress ratio and the maximum stress ratio at which failure occurs. The shading highlights 90% of the distribution, while the black lines are the 5th and 95th percentile paths (dashed) and the median path (solid) computed using a horizontal slice at $n = 500$ filaments or $\omega = 100\%$. (*b*) The histogram of times to failure shows a median rupture time of approximately 125 years.

working stress ratios to higher ones and continuous repairs. From a practical standpoint, this could be done by enhancing the climbers in [3,4] through robots capable of autonomous repair.

3.1. The case without repair

Starting with a fixed number of active filaments, corresponding to a targeted working stress ratio ω_0, we use the stochastic simulation scheme for age-structured dynamics described in §2.4 to predict the probability that the system is reliable over time. Without a repair mechanism in the system, not only is failure inevitable, but the distribution of times to failure has a large spread (figure 3). The only way one can improve reliability without repair in this framework is to decrease the operating ratio to a low enough value to delay the inevitable. This is not tenable in the space elevator, since this would require lowering the operating stress either by increasing the taper ratio to extreme values or by using materials much stronger than those currently available.

3.2. The effects of an autonomous repair mechanism

As previously mentioned, operating the space elevator segment in the absence of a repair mechanism will lead to eventual segment failures in time. We now introduce an autonomous repair mechanism, which amounts to repairing inactive filaments with a probability per unit time ρ (incidentally, an interesting optimal control problem is how to modulate ρ with the number of active filaments n most efficiently from a cost perspective). We consider the simple case of piecewise-constant repair rates with the understanding that this is not optimal. As shown in figure 4, the segment dynamics in figure 3 improve dramatically with modest repair rates (1–4 filaments every 10^4 h) by creating a bifurcation in behaviour: either filaments rupture quickly and the system fails or they last long enough for the repair rate to take over and stabilize the system. Note that, to ensure the segment mass does not increase, we do not allow the number of filaments to go above the initial value, i.e. we have a reflective barrier. This guarantees that the system is stabilized at a number of filaments corresponding to the initially targeted working stress ratio. We see that with higher repair rates, not only do we eliminate trajectories ending in failure, but we also speed up the time to reach the stable regime.

With the introduction of a repair mechanism, figure 5*a–d* shows that the system can be stabilized at significantly higher working stress ratios (the insets show histograms for the times to stabilization). This is crucial, because it implies that one can use materials with a lower UTS. The trade-off comes in the form of higher repair rates, but the scaling of repair with working stress ratio is encouraging (figure 5*e*). An additional benefit to operating at higher working stress ratios is that the system stabilizes much faster, at which point repair could be modulated down. For example, we see that, for Kevlar, operating the segment at $\omega = 90\%$ requires a repair rate $\rho = 30$ filaments per hour. Although this number may seem high, it is worth pointing out that the material flux is 3% of the segment mass every hour and that the system stabilizes in just 20 h.

We have thus found that, by adding an autonomous repair mechanism, one can ensure reliability at higher working stress ratios, which, in turn, allows for reasonable taper ratios and construction using weaker materials. In his report, Edwards [3] considers a working stress ratio of 50% and claims carbon nanotubes with σ_{max}=130 GPa would be sufficient for the cable specifications he suggests. Using recent measurements of carbon nanotube strength [14,36] of greater than 100 GPa and operating at the stress Edwards suggests implies a working stress ratio of $\omega = 65\%$. At $\omega = 65\%$, the repair rate needed for a reliable Kevlar segment would be less than $\rho = 1$ filament per hour.

3.3. Choosing minimum filament age and initial number of filaments

It is worthwhile mentioning a subtle, but consequential point regarding filament ageing. We have established that Weibull-distributed times to rupture lead to age-dependent transition probabilities per unit time of the form (2.2). If $s < 1$ in this expression (which is the case throughout this analysis), filaments will have infinite probability rates at $a = 0$. In deriving the analytic result, we assumed that newly added

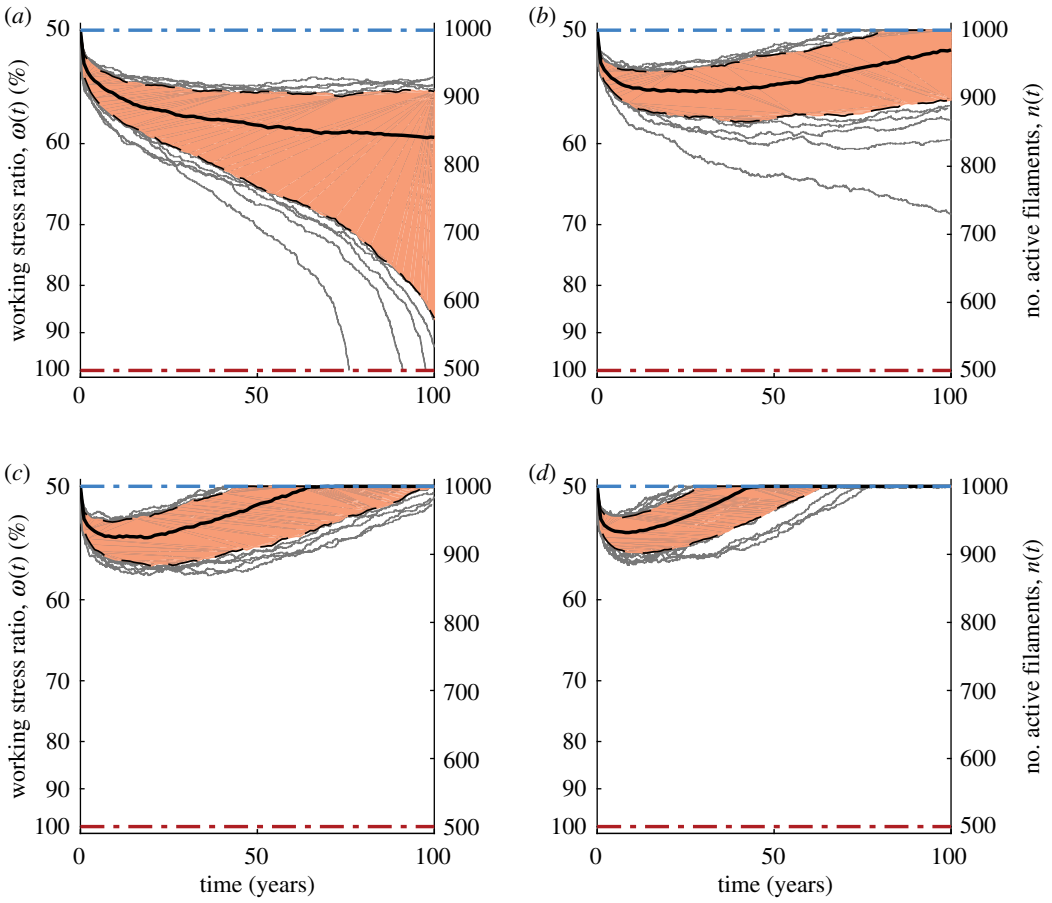

Figure 4. Effects of repair on filament dynamics and on bundle stability. A sample of 100 paths (grey) are shown for the number of filaments $n(t)$ (right) and corresponding working stress ratio $\omega(t) := \sigma(t)/\sigma_{max}$ (left). The blue and red dashed lines show the initial working stress ratio and the maximum stress ratio at which failure occurs. The shading highlights 90% of the distribution, while the black lines are the 5th and 95th percentile paths (dashed) and the median path (solid) computed using a vertical slice $t = 100$ years or at time of system stability, whichever is sooner. The repair rates are (*a*) $\rho = 10^{-4}\,\mathrm{h}^{-1}$, (*b*) $\rho = 2 \times 10^{-4}\,\mathrm{h}^{-1}$, (*c*) $\rho = 3 \times 10^{-4}\,\mathrm{h}^{-1}$ and (*d*) $\rho = 4 \times 10^{-4}\,\mathrm{h}^{-1}$.

filaments start off with age exactly $a_{min} = 0$ h. Figure 6*a* shows that the statistics obtained from the simulation are sensitive to the minimum age at small ages, but the dependency is much weaker after a few hours. Since filaments can already be stretched by the time they are installed in the segment (either as part of quality assurance, or through process of installation itself), it is reasonable to assume they will have a non-zero initial age. In simulations, we assumed $a_{min} =$ 12 h unless otherwise specified.

Another constant in the simulation is the initial number of active filaments N_0. Although the taper ratio dictates how the number of filaments in the steady state should vary along the tether, there has been no discussion so far regarding the actual number of filaments that, e.g. the base segment will have. The cross-sectional area at the base, and therefore the number of filaments, has to be sufficiently high such that, when considering the UTS of the material, the force generated compensates any additional weight on the tether, such as that of a climber or repairing robots. Consequently, the choice of N_0 has a lower bound, but is arbitrary beyond that. With $N_0 = 1000$, a material with strength 1 GPa and filament cross-sectional area $10^{-9}\,\mathrm{m}^2$ could support 1 tonne of additional weight. Beyond this, our reliability results are not overly sensitive to the numerical value of N_0 as evidenced by figure 6*b*. This is not surprising, as one can see in equation (2.3) that it is the ratio of active filaments that impacts rupture, not their nominal amount.

3.4. Comparison to analytic result

As shown in appendix A, if transition probabilities of rupture and repair do not depend on the number of active filaments n, we can obtain analytic results for first and second moments of the distribution of active filaments with ages in a given interval. We can then use the results in equation (A 5) to ensure that the stochastic simulation scheme agrees with the analytic results. In our analysis, the repair rate is a constant, but the rupture probability rate depends on stress and, therefore, analytic solutions are not straightforward. For the sake of comparing the simulation results with the analytic solutions, we will assume in this section only that the stress stays constant as filaments rupture. Physically, this would be equivalent to losing the filament when it ruptures, thus decreasing the mass and force on the segment in a manner commensurate to the loss of cross-sectional area.

We examine the dynamics of a segment starting with $N_0 = 100$ Kevlar filaments subjected to a constant stress of 3.2 GPa, leading to a working stress ratio $\omega \approx 90\%$. Here, we assume that new filaments start off with an age $a_{min} = 10^{-14}$ h. Figure 6*b* shows the comparison between the analytic expected value/standard deviation of the number of active filaments in equation (A 5) and what was obtained based on the stochastic simulation. The repair probability rate constant is taken as $\rho = 10$ filaments h^{-1}. We show 30 sample trajectories out of the 10^4 generated and used in obtaining statistics. Each trajectory was assigned a

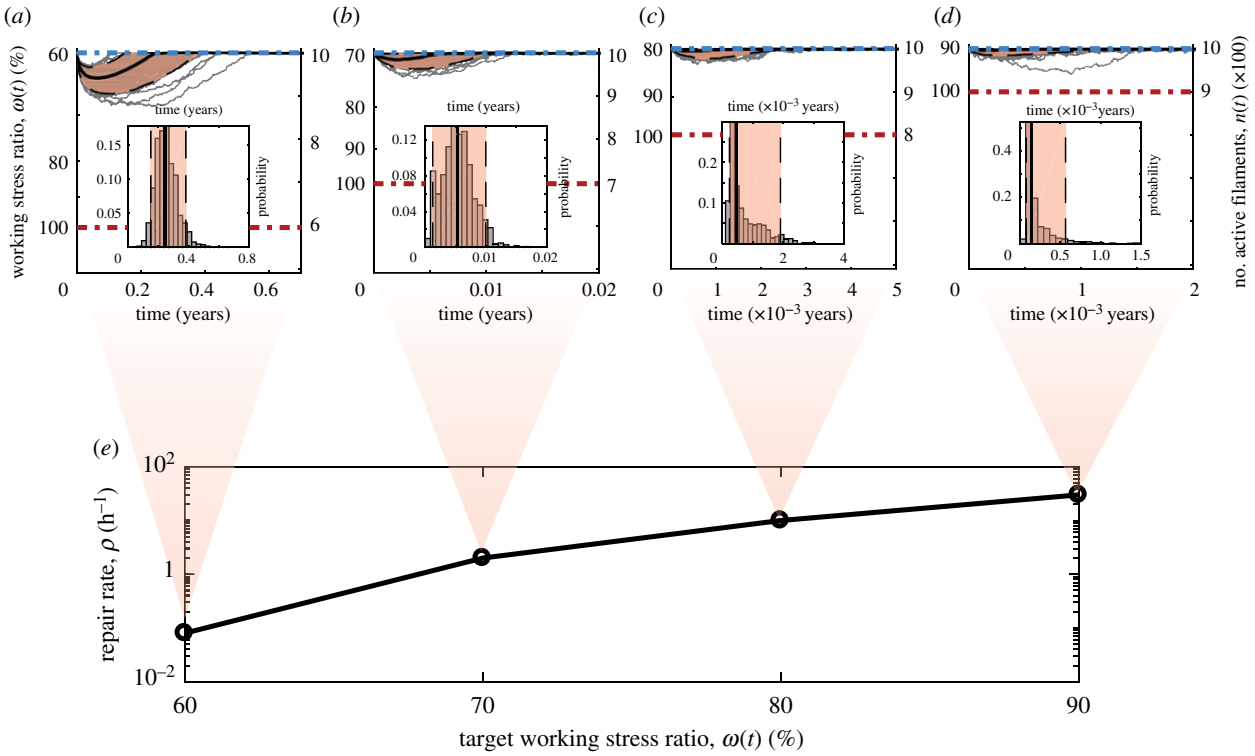

Figure 5. Target working stress ratio versus repair rate trade-off. Sample paths (grey) for number of filaments $n(t)$ (right) and working stress ratio $\omega(t) := \sigma(t)/\sigma_{max}$ (left) with corresponding 5th and 95th percentile paths (dashed) and the median path (solid), as well as shading for 90% of the distribution and stabilization time histograms (insets) are shown for different target working stress ratios and repair rates (*a*) $\omega_0 = 60\%$ and $\rho = 0.08\ h^{-1}$, (*b*) $\omega_0 = 70\%$ and $\rho = 2\ h^{-1}$, (*c*) $\omega_0 = 80\%$ and $\rho = 10\ h^{-1}$, (*d*) $\omega_0 = 90\%$ and $\rho = 30\ h^{-1}$. (*e*) Summary of the repair rates needed to sustain higher working stress ratios.

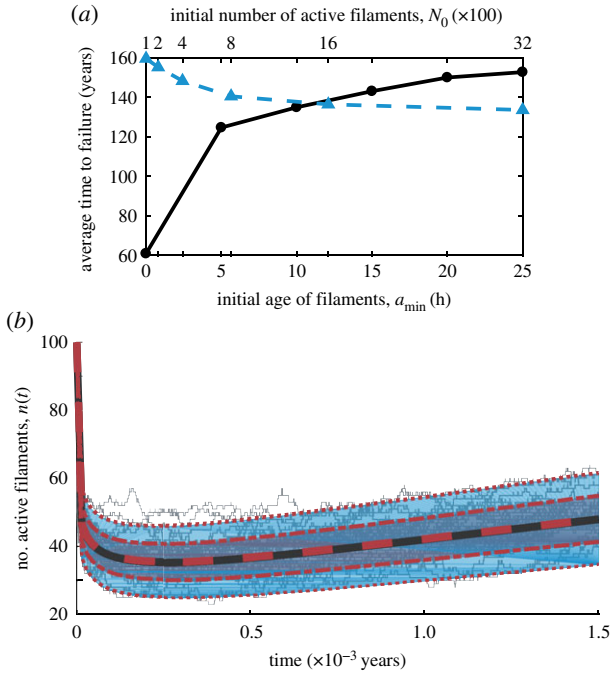

Figure 6. Age-dependent stochastic simulation. (*a*) Using the simulation scheme presented in the manuscript, we explore the sensitivity of the average time to failure to number of initial filaments (top, blue triangles, filament minimum age $a_{min} = 12$ h) and minimum age of a newly added filament (bottom, black circles, $N_0 = 1000$ initial filaments). (*b*) In the case where the stress σ is a constant, we obtain analytic results for the mean (solid black line), one standard deviation around the mean (purple shading) and two standard deviations around the mean (blue shading). We superimpose the corresponding simulated values (dashed red lines). We show 30 sample trials (grey) out of the total 10 000. The repair rate used was $\rho = 10$ filaments h^{-1} and minimum filament age of $a_{min} = 10^{-14}$ h.

maximum number of transitions (here, 400) as stopping conditions. The maximum time plotted was chosen as a predefined constant. One can see that the analytic result and the simulations are in perfect agreement.

3.5. Segment dynamics sensitivity to filament lifetime distribution

The model used in this manuscript to characterize an individual segment of the space elevator can be generalized in a few different ways. The main question the model addresses is how the stochastic lifetime of individual components translates into that of the structure built by the substructures. An important feature of the model is that the rupture probability rates of the substructures is age-dependent; that is, we combine the stochasticity of rupture times with the deterministic aspect of ageing. It turns out that this is a reasonable model for a wide-range of applications (e.g. cell division times). For the space elevator, we assume Weibull-distributed rupture times for the substructures. Additionally, we assume that the filaments building up the segment do not interact directly, i.e. they are statistically independent.

In this section, we relax the assumptions made about the lifetime distribution of the sub-components and explore the response in the lifetime distribution of the entire structure. The intention here is not to exhaust the possible distributions, but to highlight the wide applicability of the model. Alwis & Burgoyne [26] provide a comprehensive comparison of various Kevlar fibre lifetime distributions. They consider lognormal versus Weibull, as well as different functional forms for the shape and scale parameter dependency on applied stress. It was found that out of the 120 models

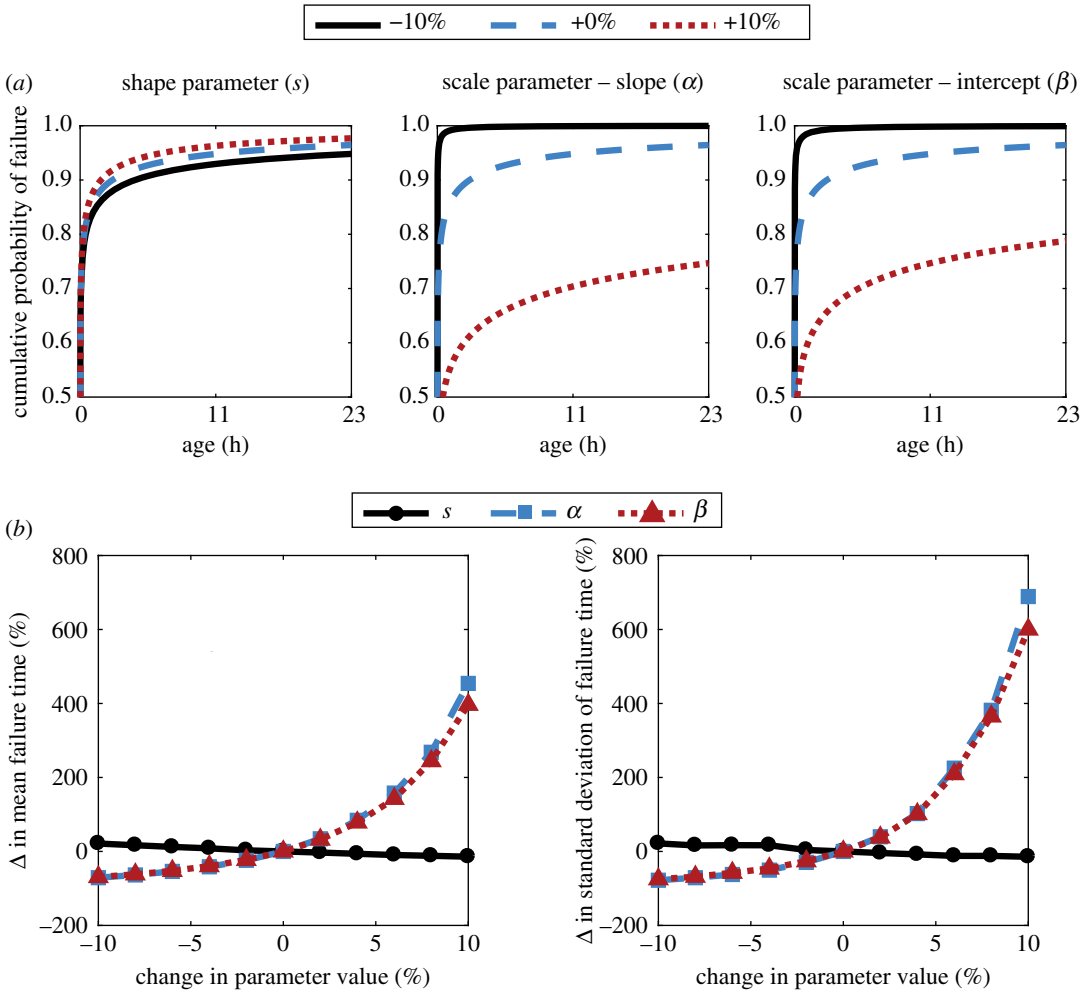

Figure 7. Dynamics sensitivity to lifetime distributions. (*a*) The shape parameter s (left) and the two scale parameters—α (middle) and β (right)—are varied to assess the resulting Weibull cumulative probability distribution. The base distribution (dashed blue line) is the one for Kevlar at $\sigma = 75\% \times \sigma_{max}$. (*b*) We analyse the response of mean and standard deviation for failure times of the segment as a percentage of their original value when the scale and shape parameters are shocked from -10% to $+10\%$ of their initial value. Again, their initial values are given by the Weibull probability of rupture for Kevlar filaments at stress $\sigma = 75\% \times \sigma_{max}$.

considered, the difference between best and worst was only 1%. Therefore, we will only focus here on varying the Kevlar-specific constants, rather than changing functional forms. That is, we start with the shape and scale parameters estimated based on [29] and seek to understand how results change when these parameters are 'shocked'.

For this analysis, we will continue to assume that each filament has an age-dependent probability of rupture given by a Weibull distribution with shape and scale parameters s and λ. We consider s a constant and λ a function of stress applied, given by $\ln(\lambda) = \alpha \ln(\sigma) + \beta$, where α and β are material constants (see §4). We varied the three parameters s, α and β from -10% to 10% of the original fitted value and analysed the response in failure time of the segment.

Figure 7*a* shows the cumulative Weibull distribution for individual filaments rupture times under different parameter shocks and values. To see how these changes impact the failure time distribution of the entire segment, one can look at figure 7*b*. We point out that changes in the shape parameter of the distribution have a significantly smaller influence than changes to the scale parameter. Since it is the latter we would expect to be different for a stronger material (being the only parameter in the model which depends on stress), this further highlights the importance of lifetime data for carbon nanotubes.

A case of particular interest is that in which the shape parameter of a Weibull distribution is equal to 1 and the distribution becomes exponential. This is particularly important when considering the filament rupture probability rate given in (2.2), which takes the form

$$k(n) = \frac{1}{\lambda(\sigma(n))}, \tag{3.1}$$

and is, therefore, independent of the filament age. In other words, we are dealing with exponentially distributed 'jump' times and one can write a master equation for the number of active filaments. Letting $P(n, t)$ be the probability that at time t the segment has n active filaments, one can write the familiar

$$\frac{\partial P(n,t)}{\partial t} = \rho P(n-1,t) + (n+1)k(n)P(n+1,t) - [\rho + nk(n)]P(n,t),$$

where ρ is the constant repair rate. The complicated dependency of k on n does not allow for straightforward analytic solutions, but one can easily perform simulations using essentially the same method described in this manuscript.

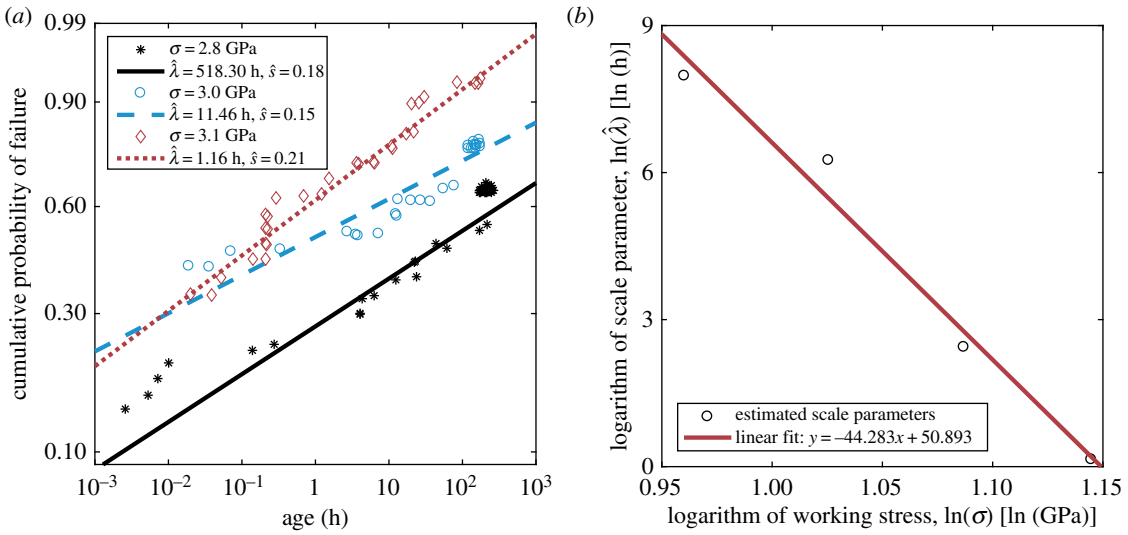

Figure 8. Creep-rupture lifetime statistics for Kevlar. Adapted from Wagner *et al*. [29]. (*a*) Lifetime data for Kevlar is shown in a Weibull plot at various stress levels: 2.8 GPa (black), 3.0 GPa (blue) and 3.1 GPa (red), together with the corresponding fitted Weibull distributions (lines). (*b*) We find an explicit dependence of the scale parameter λ on the stress σ by fitting a line of the form $\ln(\lambda) = \hat{\alpha}\ln(\sigma) + \hat{\beta}$ to the data summarized in table 2 and find $\hat{\alpha} = -44.283$ [ln (hours)/ln (GPa)] and $\hat{\beta} = -50.893$ [ln (hours)].

4. Creep-rupture lifetime data

Presently, much of the focus in carbon nanotube technology research revolves around enhancing their strength, with little emphasis on exploring their creep-rupture time distributions. Data are much more readily available for a similarly brittle fibre, namely aramid (Kevlar, manufactured by DuPont). Although the comparison is warranted in light of [35], one should be aware that defects specific to carbon nanotube structures, such as, for example, the Stone–Wales effect [37], could make their lifetime and strength distributions sufficiently different from aramid. We are not suggesting that the space elevator ought to be built using Kevlar; rather, we are aiming to draw concrete inferences on the effects of repair on the dynamics of the tether using real-world data. Encouraging results for Kevlar, a material 10 times weaker than the currently available carbon nanotubes [34], suggest that one should opt for a design which incorporates an autonomous repair mechanism.

Our choice to focus on aramid fibres is justified by the material's brittle nature and the extensive study of creep-rupture lifetime data [26–29]. It was found in Wagner *et al*. [29] that the lifetime distribution of aramid fibres under various constant stress levels is best described by a Weibull distribution with cumulative function:

$$F_W(a; \lambda, s) = 1 - \exp\left[\left(\frac{a}{\lambda}\right)^s\right], \tag{4.1}$$

where a is the age of the fibre and λ, s are the scale and shape parameters. In one of the datasets analysed, they measure rupture times of 46–48 aramid fibres subjected to stresses ranging from 2.6 to 3.1 GPa (reproduced in part in figure 8*a*) and perform a maximum-likelihood estimation of the Weibull parameters, which is summarized in table 2.

Backed by a model grounded in the theory of absolute reaction rates, the authors in [29] assume that, while s is constant, the scale parameter ln(λ) is linear in ln(σ). This is consistent with the recent analysis in [26]. We take s as constant, given by the average of the estimated shape parameters in table 2. We find an explicit dependence by fitting a line of the form $\ln(\lambda) = \hat{\alpha}\ln(\sigma) + \hat{\beta}$ to the data in table 2 and find $\hat{\alpha} = -44.283$ [ln (hours)/ln (GPa)] and $\hat{\beta} = -50.893$ [ln (hours)] (figure 8*b*). This fully determines $c_1 = s\exp(-\beta s)$ in equation (2.3).

Table 2. Shape and scale parameter estimates. (Maximum-likelihood estimators for Weibull scale $\hat{\lambda}$ and shape $\hat{s}$ parameters for filament lifetime.)

stress, σ (GPa)	scale parameter, $\hat{\lambda}$(h)	shape parameter, $\hat{s}$
2.6122	2902	0.157
2.7887	518.3	0.183
2.9652	11.46	0.146
3.1417	1.156	0.212

5. Discussion

In this manuscript, we contrasted the biological and engineering paradigms of designing complex structures. While the latter design is based on operating structures at very conservative loads compared to the strength of the materials used, thus ensuring reliability, the former allows for loads significantly closer to the maximum, but uses an autonomous and continuous repair mechanism to make up the potential loss of reliability. In megastructures, traditional engineering approaches are hampered by the necessity of prohibitively strong materials. We argue that one approach to circumvent this problem is to draw inspiration from biological structures and introduce self-repair mechanisms. In essence, this shifts the focus from requiring very strong—possibly unavailable—materials to repairing with weaker materials at the necessary rate to maintain the structure's integrity. We analysed the space elevator as an example of a megastructure and used an age-dependent stochastic model for its underlying components, which allowed us to quantitatively describe its reliability by looking at probabilities of segment failure. Results show that with sufficient repair, the space elevator is stable when operating at near 100% of the material tensile

strength. From data shown in table 1, a space elevator made of M5 is potentially feasible.

The model in this manuscript focuses primarily on the dynamics of the non-interacting sub-components (in this case, filaments) and describes how fluctuations in their number, owing to rupture and repair, translate into the reliability probability of the larger structure. Once the failure probability of a segment is understood, one can scale up the analysis in a hierarchical fashion first to the cable consisting of M segments, and then to the entire space elevator, viewed as a collection of parallel cables. Assuming segments fail independently, the survival probability of the entire cable as a function of time, $S(\tau)$, given the failure time distributions of segments, $W_j(\tau)$, is

$$S(\tau) = \prod_{j=1}^{M}\left(1 - \int_0^{\tau} W_j(t)\,\mathrm{d}t\right). \tag{5.1}$$

For a tapered cable, which implies N_0 varies along the cable, the segment failure time distribution does not vary very much (figure 6*a*). However, if other potential stochastic effects (e.g. meteors, winds and erosion) affect failure of different segments, then additional considerations may be needed to optimize N_0 and $W_j(\tau)$. We have avoided suggesting specific designs for the cable, as this was not in the scope of the manuscript. Additionally, although Kevlar was found to be strong enough to maintain reliability, its density remains prohibitively large to make it practical, given the massive volume of material which would need to be transported. On the other hand, carbon nanotubes already have the necessary strength, provided a repair mechanism can be incorporated to operate at higher working stress ratios.

Estimating the repair rates for carbon nanotubes remains an open question, contingent on the availability of data regarding their creep-rupture lifetime distribution, which has not yet been thoroughly studied to our knowledge. More research in this direction is necessary to quantify the exact requirements, but it is very encouraging to see that Kevlar, a material weaker by an order of magnitude compared with the theoretically predicted strength of carbon nanotubes, can operate reliably without much material turnover. Incidentally, the inferences drawn from our model have biological applications: while healing, tendons remain under tension owing to cells exerting active forces to stretch the collagen, similar to how repairing robots would stretch the filaments in the space elevator. This allows for a better understanding of the dynamics of biological repair, with possible applications to many different structures (e.g. bones, tendons and muscle). Furthermore, our analysis provides the necessary framework to consider more complex models in which filaments can interact, material strengths are stochastic and external noise on the cable is present. We also emphasize that piecewise-constant repair probability rates are overly-conservative. More complicated control theory approaches can significantly increase feasibility by lowering the amount of repair needed as structures stabilize.

Data accessibility. All data needed to evaluate the conclusions in the paper are present in the manuscript. Additional data and code related to this paper may be requested from the authors.

Authors' contributions. D.M.P. and S.X.S. conceived the research, designed and conducted the analyses and wrote the manuscript.

Competing interests. We declare we have no competing interests.

Funding. This work was supported by The Johns Hopkins University President's Frontier Award.

Acknowledgements. The authors thank Benjamin W. Schafer for helpful conversations. The authors also thank Jenna Powell-Malloy for illustrating the space elevator cartoon.

Appendix A. Moment equations for the number of filaments

In the special case in which the repair and rupture rates do not depend on the number of active filaments n, a hierarchy for the moments can be written explicitly and solved analytically starting with (2.1). For example, this occurs when $n \approx N_0$, the initial number of active filaments, given that the total segment force and, hence, $\sigma(t) \times n(t)$ are approximated as constant. While these approximations depend on various material-specific factors, we include the analysis with the understanding that it is relevant in special cases, particularly when the segment is close to its targeted working stress ratio, ω_0. Moreover, it serves as good validation of the simulation scheme. Let $k_n(a_i) \equiv k(a_i)$, $\rho_n \equiv \rho$, and define the marginal j-dimensional distribution function as in [31]:

$$p_n^{(j)}(\boldsymbol{a}_j;\, t) \equiv \int_0^{\infty} \mathrm{d}a_{j+1} \ldots \int_0^{\infty} \mathrm{d}a_n p_n(\boldsymbol{a}_n;\, t), \tag{A 1}$$

and the factorial moments as

$$X^{(j)}(\boldsymbol{a}_j;\, t) \equiv \sum_{n=j}^{\infty} \frac{n!}{(n-j)!} p_n^{(j)}(\boldsymbol{a}_j;\, t), \tag{A 2}$$

for $j \geq 1$ and we set $X^{(0)} \equiv 1$. Successively integrating equation (2.1) and its conditions over $n - j$ (non-zero) age variables and summing over all $n \geq j$, we can now write and solve the moment equations:

$$\frac{\partial X^{(j)}(\boldsymbol{a}_j;\, t)}{\partial t} + \sum_{i=1}^{j} \frac{\partial X^{(j)}(\boldsymbol{a}_j;\, t)}{\partial a_i} + X^{(j)}(\boldsymbol{a}_j;\, t) \sum_{i=1}^{j} k(a_i) = 0 \tag{A 3a}$$

$$X^{(j)}(\boldsymbol{a}_{j-1},\, 0;\, t) = \rho X^{(j-1)}(\boldsymbol{a}_{j-1};\, t) \tag{A 3b}$$

and

$$X^{(j)}(\boldsymbol{a}_j;\, t = 0) = g^{(j)}(\boldsymbol{a}_j). \tag{A 3c}$$

To make the problem concrete, we derive explicit forms for the initial conditions $g^{(j)}(\boldsymbol{a}_j)$. Assume the cable segment starts off with N_0 initial number of filaments, all with age 0. Then, $p_n(\boldsymbol{a}_n;\, t = 0) = \delta_{n,N_0} \prod_{l=1}^{n} \delta(a_l)$, where $\delta_{i,j}$ is the Kronecker delta and $\delta(\cdot)$ is the Dirac delta function. From (A 1) and (A 2), we find

$$g^{(j)}(\boldsymbol{a}_j) = \frac{N_0!}{(N_0 - j)!} \prod_{l=1}^{j} \delta(a_l). \tag{A 4}$$

We note that, for $j = 1$, equation (A 3*a*) reduces to the classic McKendrick–von Foerster equation [38,39], which can easily be solved via the method of characteristics [31]. We find for the first two moments:

$$X^{(1)}(a_1;t) = \begin{cases} N_0 \delta(a_1 - t) U(a_1 - t,\, a_1) & (a_1 \geq t) \\ \rho U(0,\, a_1), & (a_1 < t) \end{cases}$$

$$X^{(2)}(a_1, a_2;t) = \begin{cases} N_0(N_0 - 1) \prod_{l=1}^{2} \delta(a_l - t) U(a_l - t,\, a_l) & (t < a_1 < a_2) \\ N_0 \rho \delta(a_2 - t) U(0, a_1) U(a_2 - t,\, a_2) & (a_1 < t < a_2) \\ \rho^2 U(0, a_1) U(0,\, a_2) & (a_1 < a_2 < t), \end{cases}$$

where the propagator is $U(a,b) \equiv \exp[-\int_a^b k(\alpha)\mathrm{d}\alpha]$ and only the cases $a_1 < a_2$ were considered, given that the moments are invariant in the ordering of the age arguments. As shown in [40], if we let $n_{[a_1,a_2]}(t)$ be the random variable representing the number of filaments with ages in the interval $[a_1, a_2]$, we have $\langle n_{[a_1,a_2]}(t) \rangle = \int_{a_1}^{a_2} X^{(1)}(u;t)\mathrm{d}u$ and $\langle n^2_{[a_1,a_2]}(t) \rangle = \int_{a_1}^{a_2} X^{(1)}(u;t)\mathrm{d}u + \int_{a_1}^{a_2}\int_{a_1}^{a_2} X^{(2)}(u,v;t)\mathrm{d}u\mathrm{d}v$, and for

$a_1 < t < a_2$, we get for the expectation and variance:

$$\left.\begin{aligned} &En_{[a_1,a_2]}(t) = N_0 U(0,t) + \rho W(a_1,t) \\ \text{and}\quad &\operatorname{Var} n_{[a_1,a_2]}(t) = N_0 U(0,t)[1-U(0,t)] + \rho W(a_1,t), \end{aligned}\right\} \quad \text{(A5)}$$

where the integral of the propagator is $W(a,b) = \int_a^b U(0,\alpha)\,\mathrm{d}\alpha$. If we now let $a_1 \to 0$ and $a_2 \to \infty$, we get the total expected number of filaments and their fluctuations.

References

1. Tsiolkovsky KE. 2004 *Dreams of earth and sky*, 1895, reissue. Barcelona, Spain: Athena Books.
2. Audacious and outrageous: space elevators. 2000 See https://science.nasa.gov/science-news/science-at-nasa/2000/ast07sep_1 (cited 9 January 2017).
3. Edwards B. 2001 The space elevator: NIAC phase I report. See http://www.niac.usra.edu/files/studies/final_report/472Edwards.pdf (cited 9 January 2017).
4. Edwards B. 2003 The space elevator: NIAC phase II final report. See http://keithcu.com/wiki/images/6/67/Edwards_NIAC_Phase_II.pdf (cited 9 January 2017).
5. Maquirriain J. 2011 Achilles tendon rupture: avoiding tendon lengthening during surgical repair and rehabilitation. *Yale J. Biol. Med.* **84**, 289–300.
6. Granhed H, Jonson R, Hansson T. 1987 The loads on the lumbar spine during extreme weight lifting. *Spine* **12**, 146–149. (doi:10.1097/00007632-198703000-00010)
7. Taylor D, Hazenberg J, Lee T. 2007 Living with cracks: damage and repair in human bone. *Nat. Mater.* **6**, 263–268. (doi:10.1038/nmat1866)
8. Gordon J. 1988 *The new science of strong materials (or why you don't fall through the floor)*, 2nd edn. Princeton, NJ: Princeton University Press.
9. Isaacs JD, Vine AC, Bradner H, Bachus GE. 1966 Satellite elongation into a true 'sky-hook'. *Science* **151**, 682–683. (doi:10.1126/science.151.3711.682)
10. Pearson J. 1975 The orbital tower: a spacecraft launcher using the Earth's rotational energy. *Acta Astronaut.* **2**, 785–799. (doi:10.1016/0094-5765(75)90021-1)
11. Aravind P. 2007 The physics of the space elevator. *Am. J. Phys.* **75**, 125–130. (doi:10.1119/1.2404957)
12. Bai Y *et al.* 2018 Carbon nanotube bundles with tensile strength over 80 GPa. *Nat. Nanotechnol.* **13**, 589–595. (doi:10.1038/s41565-018-0141-z)
13. Cunniff PM, Auerbach MA, Vetter E, Sikkema DJ. 2002 High performance 'M5' fiber for ballistics/structural composites. In *23rd Army Science Conf.*, *Citeseer*, 2–5 December 2002, Orlando, FL, p. 1e8.
14. De Volder M, Tawfick S, Baughman R, Hart A. 2013 Carbon nanotubes: present and future commercial applications. *Science* **339**, 535–539. (doi:10.1126/science.1222453)
15. Islam MS, Deng Y, Tong L, Faisal SN, Roy AK, Minett AI, Gomes VG. 2016 Grafting carbon nanotubes directly onto carbon fibers for superior mechanical stability: towards next generation aerospace composites and energy storage applications. *Carbon* **96**, 701–710. (doi:10.1016/j.carbon.2015.10.002)
16. Pugno N. 2013 Towards the Artsutanov's dream of the space elevator: the ultimate design of a 35 GPa strong tether thanks to graphene. *Acta Astronaut.* **82**, 221–224. (doi:10.1016/j.actaastro.2012.01.008)
17. Riley G. 2003 The pathogenesis of tendinopathy. A molecular perspective. *Rheumatology* **43**, 131–142. (doi:10.1093/rheumatology/keg448)
18. Daniels H. 1945 The statistical theory of the strength of bundles of threads. I. *Proc. R. Soc. Lond. A* **183**, 405–435. (doi:10.1098/rspa.1945.0011)
19. Coleman B. 1956 Time dependence of mechanical breakdown phenomena. *J. Appl. Phys.* **27**, 862–866. (doi:10.1063/1.1722504)
20. Coleman B. 1957 A stochastic process model for mechanical breakdown. *Trans. Soc. Rheol.* **1**, 153–168. (doi:10.1122/1.548812)
21. Coleman B. 1958 Statistics and time dependence of mechanical breakdown in fibers. *J. Appl. Phys.* **29**, 968–983. (doi:10.1063/1.1723343)
22. Phoenix S. 1978 The asymptotic time to failure of a mechanical system of parallel members. *SIAM J. Appl. Math.* **34**, 227–246. (doi:10.1137/0134021)
23. Phoenix S. 1979 The asymptotic distribution for the time to failure of a fiber bundle. *Adv. Appl. Prob.* **11**, 153–187. (doi:10.2307/1426773)
24. Newman W, Phoenix S. 2001 Time-dependent fiber bundles with local load sharing. *Phys. Rev. E* **63**, 021507. (doi:10.1103/PhysRevE.63.021507)
25. Phoenix S, Newman W. 2009 Time-dependent fiber bundles with local load sharing. II. General Weibull fibers. *Phys. Rev. E* **80**, 066115. (doi:10.1103/PhysRevE.80.066115)
26. Alwis K, Burgoyne C. 2005 Statistical lifetime predictions for aramid fibers. *J. Compos. Const.* **9**, 106–116. (doi:10.1061/(ASCE)1090-0268(2005)9:2(106))
27. Phoenix S, Beyerlein I. 1992 Modelling the fatigue strength and lifetime of wires and cables. *IABSE Reports* **80**, 99–110. (doi:10.5169/seals-50689)
28. Phoenix S, Schwartz P, Robinson H. 1988 Statistics for the strength and lifetime in creep-rupture of model carbon/epoxy composites. *Compos. Sci. Technol.* **32**, 81–120. (doi:10.1016/0266-3538(88)90001-2)
29. Wagner H, Schwartz P, Phoenix S. 1986 Lifetime statistics for single Kevlar 49 filaments in creep-rupture. *J. Mater. Sci.* **21**, 1868–1878. (doi:10.1007/BF00547921)
30. Greenman C, Chou T. 2016 Kinetic theory of age-structured stochastic birth-death processes. *Phys. Rev. E* **93**, 012112. (doi:10.1103/PhysRevE.93.012112)
31. Chou T, Greenman C. 2016 A hierarchical kinetic theory of birth, death and fission in age-structured interacting populations. *J. Stat. Phys.* **164**, 49–76. (doi:10.1007/s10955-016-1524-x)
32. Callister WD, Rethwisch DG. 2011 *Materials science and engineering*, vol. 5. New York, NY: John Wiley & Sons.
33. Gillespie D. 1992 *Markov processes: an introduction for physical scientists*. San Diego, CA: Academic Press.
34. Barber A, Andrews R, Schadler L, Wagner H. 2005 On the tensile strength distribution of multiwalled carbon nanotubes. *Appl. Phys. Lett.* **87**, 203106. (doi:10.1063/1.2130713)
35. Yang L, Greenfeld I, Wagner H. 2016 Toughness of carbon nanotubes conforms to classic fracture mechanics. *Sci. Adv.* **2**, e1500969. (doi:10.1126/sciadv.1500969)
36. Peng B, Locascio M, Zapol P, Li S, Mielke S, Schatz G, Espinosa HD. 2008 Measurements of near-ultimate strength for multiwalled carbon nanotubes and irradiation-induced crosslinking improvements. *Nat. Nanotechnol.* **3**, 626–631. (doi:10.1038/nnano.2008.211)
37. Stone A, Wales D. 1986 Theoretical studies of icosahedral C60 and some related species. *Chem. Phys. Lett.* **128**, 501–503. (doi:10.1016/0009-2614(86)80661-3)
38. M'Kendrick A. 1925 Applications of mathematics to medical problems. *Proc. Edinb. Math. Soc.* **44**, 98–130. (doi:10.1017/S0013091500034428)
39. von Foerster H. 1959 *Some remarks on changing populations in the kinetics of cell proliferation*. Berlin, Germany: Springer.
40. Greenman C. 2017 A path integral approach to age dependent branching processes. *J. Stat. Mech: Theory Exp.* **2017**, 033101. (doi:10.1088/1742-5468/aa4f16)